Publications of the Astronomical Society of the Pacific
108: 699–705, 1996 August

The Telescopic Point-Spread Function

RENÉ RACINE

Département de physique, Université de Montréal and Observatoire astronomique du mont Mégantic, Montréal, Canada H3C 3J7
Electronic mail: racine@astro.umontreal.ca

Received 1996 March 13; accepted 1996 May 20

ABSTRACT. New observations are used to accurately define the stellar point-spread function produced by atmospheric turbulence at the focus of large telescopes and to compare its profile to those computed from wave fronts characterized by various structure functions. Excellent agreement is found with the PSF expected from Kolmogorov statistics, except for the presence of an extended aureole of light which appears to result from a combination of instrumental and atmospheric light scattering. Simple yet accurate analytical fits are developed to represent the PSF profile over a range of 15 magnitudes in surface brightness. The relation between the Strehl ratio S of the PSF and the value of the parameter D/r_0 is rediscussed, both for a natural wave front and for a wave front whose variance Δ_N is reduced by an adaptive optics systems. A simple expression for $S(D/r_0,\Delta_N)$ is proposed and shown to yield essentially correct Strehl ratios for any value of the parameters.

1. INTRODUCTION

Twenty-five years ago, Ivan King (1971) was able to derive the radial intensity profile of a stellar image over a range of 27 magnitudes, a factor of $\sim 10^{11}$ in surface brightness. This feat was accomplished by combining data from photographic stellar images on a Palomar Observatory Sky Survey plate and on plates taken at the Mount Wilson 60-in telescope, supplemented by measurements of the sky brightness near the Sun (van de Hulst 1952). The point-spread function (PSF) was found to be composed of an exponential core superposed on an θ^{-2} aureole, first noted by de Vaucouleurs (1958), which dominates beyond $\theta \sim 10$ HWs (HW: half full width at half peak intensity).

With the advent of photometrically accurate panoramic detectors of large dynamic range, such as CCDs and infrared arrays, one might have expected a similar investigation, of possibly greater precision, to have been repeated and published. This has apparently not been done, possibly because of concerns that instrumental or local effects, such as telescopic aberrations and "dome seeing," might make the results, however precise, too specific to be of broad utility. But the question still remains of interest. An accurate yet simple parameterization of the PSF is helpful in image analysis software packages such as DAOPHOT (Stetson 1987). More importantly perhaps, since the shape of the PSF is related to the form of the structure function or modulation transfer function (MTF) of the atmosphere (Johnson 1973; Woolf 1982), it can serve as a test of atmospheric turbulence models. Finally, and what first prompted this author to revisit this issue, the empirical relation between the Strehl ratio, or central intensity, of a stellar PSF and its HW depends on its actual overall profile, through flux conservation considerations. This is in turn related to the evaluation of performances for adaptive optics (AO) systems, a topic of considerable current interest in astronomy (Beckers 1993). In particular, a convenient yet precise approximation relating the Strehl ratio of an AO compensated PSF to the strength of the atmospheric turbulence and the level of compensation would be a useful tool in such evaluations.

In this paper, new CCD and IR observations of stellar PSFs are presented and compared to King's results. These data are then compared to the profiles expected from various atmospheric MTFs. This step amplifies, with data of greater precision, earlier discussions by Roddier (1981) and by Woolf (1982). An analytically simple yet remarkably accurate fit to the atmospheric PSF is developed and used to relate its Strehl ratio to the phase variance of the atmospheric wave front. Finally, this Strehl-variance relation is extended to wave fronts partially compensated by an adaptive optics system.

2. DATA

Stellar images obtained in the B band (λ=0.44 μm) with a 0.18 arcsec pixel^{-1} CCD imager at the Cerro Tololo Inter-American Observatory 1.5-m telescope in 1995 October, and in the H band (λ=1.65 μm) with a 0.20 arcsec pixel^{-1} IR camera at the Mont Mégantic Observatory 1.6-m telescope in 1995 July were culled from archives and analyzed. The images selected were taken under excellent photometric skies when atmospheric turbulence was strong, as indicated by poor seeing (HW $\sim$1.5 arcsec) at all CTIO telescopes, for instance. This ensures low atmospheric diffusion and minimal signatures from telescopic aberrations. They were relatively short exposures focus tests (10–20 s, which is sufficient to average the speckle pattern and small-scale seeing fluctuations), taken under calm wind conditions, to ensure good focus and to minimize smear from telescope vibrations and tracking errors. The frames were closely examined for evidence of detectable close companions to the PSF star, or of any irregularities such as image elongation, low-intensity flares other than the diffraction spikes from the secondary mirror support, or background unevenness after division by flat-field exposures. A very small fraction of the available archival images satisfied all of these selection criteria. In the

end, two CCD images and two IR images were chosen for analysis.

After bias and dark signal subtractions, flat-fielding and interpolative corrections for bad pixels, the sky was subtracted from the frames. Its level was estimated from the mode of pixel values well away from the PSF star (>70 HWs) on the 2K×2K CCD frames and from blank sky exposures with the narrower field IR camera. Four radial subarrays of pixels corresponding to the (barely detectable) diffraction spikes were excised from the frames beyond 2 HWs of the PSF star center. The radial intensity profiles were extracted with the IRAF task PRAD and normal points were computed. The intensities of the individual profiles were normalized to their central values, estimated by a simple extrapolative fit, and the radii were normalized to their interpolated HW values. Each profile had sufficient statistics to define the shape of the PSF out to a radius of ~10 HWs, spanning a dynamic range of ~9 magnitudes (~4000×) in surface brightness, with a precision better than 3%. Comparison of the profiles showed no significant differences in shape at that level of precision. Thus, the four profiles were averaged, equal weight being given to each one. The HW estimate for this mean PSF is formally accurate to ±3%.

Since the images were taken at different sites, with different telescopes and different auxiliary optics, the good agreement between the profiles suggests that instrumental aberrations and light scattering by the optics and within the detectors do not significantly modify the shape of these inner PSFs produced by atmospheric turbulence and diffusion. The agreement between the profiles in *B* and in *H* also shows that the PSF *shape* is independent of wavelength under conditions well away from the telescope diffraction limit, which was certainly the case when these observations were taken. This is as expected from seeing theory.

A few nights after the CTIO 1.5-m telescope images were obtained, in a totally unrelated project, a mosaic CCD imager was used at the prime focus of the Blanco 4-m telescope to map the sky brightness in *B* around a ninth magnitude SAO star (A. Tyson, private communication). The star itself was placed just off the CCD pixel array, to avoid gross saturation, and a 500-s exposure allowed to map the profile of the outer seeing disk and PSF aureole out to a radius of 200 arcsec and to a flux level of ~29 mag arcsec^{-2}. These data, which may have been affected by the suspected presence of very thin cirrus, largely overlap the radii covered by the central PSF profile and will be used to extend its shape over a total range of ~18 mag (~2×10^7).

3. THE OBSERVED PSF

In Fig. 1, the present PSF profile is compared to the one obtained by King, also normalized in intensity and radius. The overall shapes are seen to be very similar and the flattening of the central exponential profile beyond θ~10 HWs is apparent in both profiles. In the PSF core, the agreement between the shapes defined by the higher-resolution frames and by the Tyson data is excellent. They both follow closely the ridge line of the King data, albeit with significantly less scatter, as expected from the higher precision which CCDs and IR arrays allow. There appears to be a significant offset between the photographic and electronic profiles at ~10<θ/HW<~100. The reason for this will become clearer when the nature of the aureole is discussed in Sec. 5.2. On the other hand, the fact that the dynamic range which King was able to cover with photographic techniques is larger than that of the present electronic profile by a factor of ~10^4 (!) inspires a certain amount of respect for clever uses of "old" technologies.

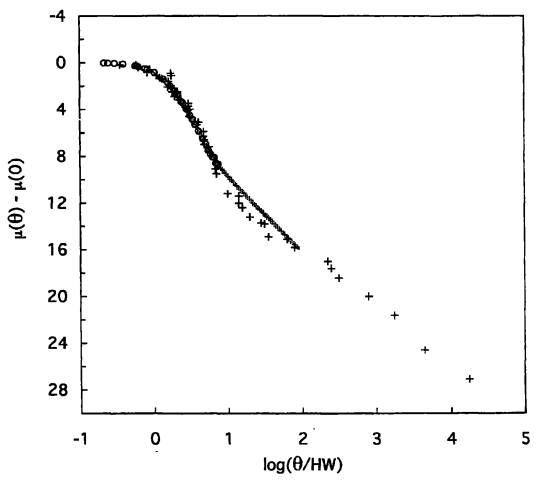

FIG. 1—The "electronic" PSF (circles to which the stippled line, adapted from Tyson's data, has been fitted) is compared to the photographic results obtained by King (1971) (crosses). The ordinate is in magnitudes.

The agreement between the shapes of the inner PSFs obtained under vastly different conditions and by quite different techniques confirms that they result from atmospheric phenomena whose effects, apart from scale factors removed by the normalization procedure, remain stationary. As will be shown below, the shape of the inner PSF can be reproduced by standard models of atmospheric turbulence. But the shallow aureole cannot. Its explanation in terms of atmospheric diffusion (van de Hulst 1981) or by the scattering of light by telescopic or instrumental optics remains somewhat conjectural.

4. THE THEORETICAL PSF

Formally, for an arbitrarily large telescope aperture, the long-exposure PSF profile $I(\theta)$ is the Bessel transform of the long-exposure atmospheric MTF $[T(\omega)]$ whose form may be written (Johnson 1973)

$$T(\omega)=\exp[-(\omega/\omega_c)^n]=\exp[-\tfrac{1}{2}\mathscr{D}(\omega/\omega_c)]. \quad (1)$$

$\mathscr{D}(\omega/\omega_c)$ is the structure function of the atmospheric wave front (Fried 1966b) and ω is the spatial frequency in the telescope focal plane in units of ω_c, which may be chosen as radians of phase per unit length (e.g., $2\pi/\lambda$) or, multiplying by a suitable length l, as radians per radian field of view. The parameter n is the structure function index. Writing $I(\theta)$ in units of ω_c^{-2}, one has

$$I(\theta)=\int_0^\infty J_0(\omega\theta)\exp\left[-\left(\frac{\lambda\omega}{2\pi l}\right)^n\right]\omega\, d\omega. \quad (2)$$

TABLE 1
Normalized PSF Profile for the MTF $\exp[-(\omega/\omega_c)^{5/3}]$

$\theta\omega_c$	$I(\theta)$	$\theta\omega_c$	$I(\theta)$
0.0	1.00+0	5.0	7.73−3
0.2	9.85−1	6.0	3.39−3
0.4	9.46−1	7.0	1.74−3
0.7	8.48−1	8.0	1.01−3
1.0	7.71−1	9.0	6.26−4
1.46	5.00−1	10.0	4.07−4
2.0	2.85−1	20.0	2.61−5
3.0	8.02−2	50.0	6.59−7
4.0	2.23−2		

Closed-form analytical solutions for $I(\theta)$ can be obtained for integer values of n. For $n=0$ (uniform response at all spatial frequencies), $I(\theta)$ is essentially the Dirac delta function and the PSF is infinitely narrow. For $n=1$, the PSF is a Lorentzian, $(1+\omega_c^2\theta^2)^{-3/2}$, and for a Gaussian MTF ($n=2$) the PSF is also a Gaussian, $\exp[-(\omega_c\theta/2)^2]$. The MTF is physically unrealizable for $n>2$ since it would lead to $I(\theta)<0$ for large values of $\omega_c\theta$.

For an atmosphere whose turbulent structure can be characterized by Kolmogorov statistics, $n=5/3$ (Tatarski 1961; Fried 1965, 1966a). In his pivotal paper, Fried (1966b) defines a quantity r_0 to measure the separation r between two points in the entrance pupil such that

$$\mathscr{D}(r/r_0)=6.8839(r/r_0)^{5/3}=6.8839\left(\frac{\lambda}{2\pi}\frac{\omega}{r_0}\right)^{5/3}. \quad (3)$$

This sets

$$\omega_c=\frac{2\pi}{2.0993}\left(\frac{r_0}{\lambda}\right). \quad (4)$$

Johnson (1973) gives a table of $I(\theta)$ for $1\leq n\leq 2$ in steps of 0.1 and for $0\leq\theta\omega_c\leq 10$ in unit steps. A detailed comparison with the observed PSF requires a higher resolution at small values of $\theta\omega_c$ as well as an extension to larger values and specifically for the case $n=5/3$. Equation (2) was numerically integrated for $n=5/3$ and $0\leq\theta\omega_c\leq 50$. The results, normalized to $I(0)=0.551$, are given in Table 1. The PSF falls to its half central intensity point at $\theta_{1/2}\omega_c=1.46$. Hence, by Eq. (4), for Kolmogorov turbulence,

$$\mathrm{FWHM}\equiv 2\ \mathrm{HW}=0.976\frac{\lambda}{r_0}. \quad (5)$$

The observed PSF is compared to the theoretical profiles for $n=1$, 5/3, and 2 in Fig. 2. Only the higher-precision electronic observations are shown. The data points follow closely the profile expected from a Kolmogorov turbulence out to a radius of ~10 HWs, which covers a factor of ~4000 in surface brightness. There is excellent agreement in Fig. 2 between the slopes defined by the data from the CTIO 4-m telescope (stippled line) and from the CTIO 1.5-m and the Mégantic 1.6-m telescopes (open circles). The traditional Gaussian ($n=2$) is not a good fit to real atmospheric PSFs: it has too little power at large radii. Beyond 10 HWs, the Kolmogorov profile lies increasingly below the PSF aureole. The King profile (see Fig. 1) would follow the $n=5/3$ curve some

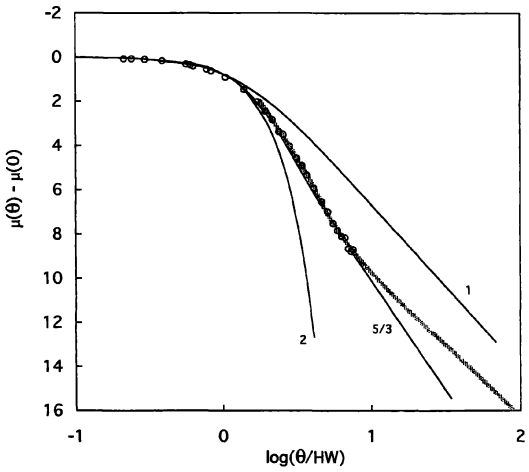

FIG. 2—The observed PSF (open circles, stippled line) is compared to theoretical models for MTFs of different indices n.

4 mag further before merging into the aureole. The observed profile appears to be slightly (~4%) wider than the model around $\mu(\theta)-\mu(0)\sim 5$ mag ($I/I_0\sim 10^{-2}$) but this is barely more than the uncertainty on the estimate of its HW. Diffraction at the pupil edge and by the secondary mirror obstruction, which is neglected in Eq. (2), must also contribute to a slight broadening of the PSF wings.

Roddier (1981) noted that the core of the PSF, as measured by King, was fitted well with a wave-front disturbance which resulted from Kolmogorov turbulence. In addition, Roddier pointed out that a finite inner scale of turbulence would enhance the PSF power at large offsets by diffracting light at large distances. Turbulent energy is, however, believed to decay into heat at the molecular scale. Rayleigh scattering by atmospheric gases is independent of the phase angle. It appears that the origin of the aureole cannot be attributed to atmospheric turbulence.

5. AN ANALYTICAL FIT TO THE PSF

5.1 The Kolmogorov Profile

For a number of practical applications such as image simulations or PSF fitting in image analysis, a simple yet precise closed-form expression for the PSF would be more convenient to use than the integral of Eq. (2). Gaussian fits, despite their inadequacy, are still used. The latest version of the DAOPHOT software (Stetson et al. 1990; Stetson 1994) also allows the use of Moffat functions (Moffat 1969). Their form is

$$I(\theta)=\frac{I_0}{(1+(\theta/R)^2)^\beta}=\frac{1}{\pi\,\mathrm{HW}^2}\frac{(2^{1/\beta}-1)(\beta-1)F}{(1+(2^{1/\beta}-1)(\theta/\mathrm{HW})^2)^\beta}, \quad (6)$$

where F is the total flux and the index β controls the strength of the PSF wings. When $\beta\to\infty$, the Moffat function becomes a Gaussian.

Figure 3 shows the Kolmogorov PSF fitted by a single Moffat function of same HW and $\beta=4$, and by the sum of two Moffat functions having the same HWs, one with $\beta_1=7$

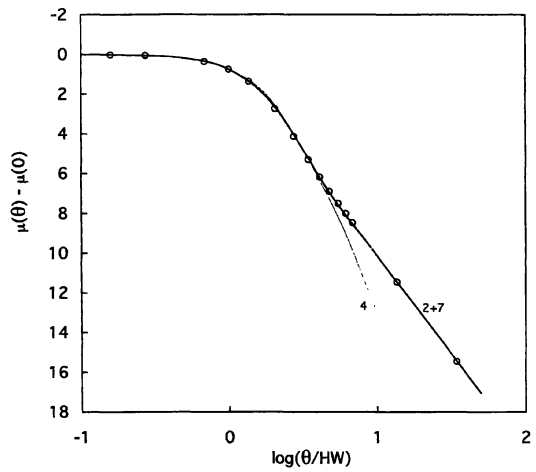

FIG. 3—The Kolmogorov PSF (open circles) fitted by a Moffat function with β=4 (thin line) and by the sum of two Moffat functions (β_1=7 and β_2=2). All functions have the same HW as the PSF.

containing 80% of the total flux and contributing 86% to the central intensity, and the other with β_2=2. Note that the fluxes quoted correspond to the integral of the profiles to infinite radii. For the θ^{-2} aureole of the King PSF (Fig. 1), that integral diverges. The single function fit is good over a range of ~7 mag in surface brightness; the two-function model provides a good fit over more than 15 mag (10^6).

5.2 The Aureole

Previous observations of the outer PSF profile (de Vaucouleurs 1948, 1958; van de Hulst 1952; King and Hinrichs 1967; Moffat 1969; Kormendy 1973; King 1971) have prompted a number of speculations on its origin. Besides well-understood diffraction effects caused by the pupil geometry, light scattering by atmospheric aerosols, or by scratches, microripples or dust on the telescope optics have been identified as the most likely culprits (van de Hulst 1952, 1981). Roddier and Roddier (1993) and Roddier (1995) have indeed shown by computer simulations that the θ^{-2} falloff can be closely approximated by the intensity scattered from a realistic spectrum of optical surface microripples. A comprehensive list of contributors to the aureole is given and discussed by Beckers (1995). At large offsets, the intensity of θ-dependent terms is found to be dominated by that from microripple and dust scattering whose effects Beckers assumes to be proportional to θ^{-2}.

The PSF aureole may also be caused, in part, by the diffusion and reflection of light within the detector assembly. The spot of light which forms the PSF must act as a diffuse source. Some of that light can be returned to the detector by reflection on another (glass?) surface.

Let F be the total flux detected in the PSF, aureole excluded, and fF the flux which is returned to the detector by diffusion and reflection. The fraction f depends on the diffuse reflectivity of the surface on which the PSF is formed, assumed to have an isotropic phase function in 2π steradians, and on the coefficient of specular reflection k_r of the (glass?) surface. If the distance between the diffuse source and the reflecting surface is d_0 in HW units, the surface brightness of the diffuse aureole can be written

$$I(\theta)=\frac{fF}{8\pi d_0^2}\cos^3\left(\text{atan}\left(\frac{\theta}{2d_0}\right)\right). \quad (7)$$

Figure 4 shows that the addition of an aureole described by Eq. (7) to the Kolmogorov PSF can adequately represent the full PSF defined by King's photographic data and the one from the present CCD data. The parameters of the fit (d_0/HW;f) are (100±30; 0.03±0.01) for the King data and (10±2; 0.020±0.005) for the CCD data. For the King photographic data, the value of d_0/HW leads to d_0~1 mm, which is the thickness of a Palomar Schmidt plate. The value of f appears reasonable given a coefficient of diffusion of ~0.5 for the emulsion and a reflectivity of ~0.04 for a glass surface. The Tyson CCD data lead to d_0~0.5 mm; this does not correspond to the distance of any surface above or behind the detector: the cryostat window, the nearest surface, is ~10 mm away. This brighter aureole may have been caused by thin cirrus clouds. Although this numerology does not prove that the PSF aureole is partly an instrumental effect—the experimental results are too ambiguous—it leads one to suspect that this may have been the case for photographic

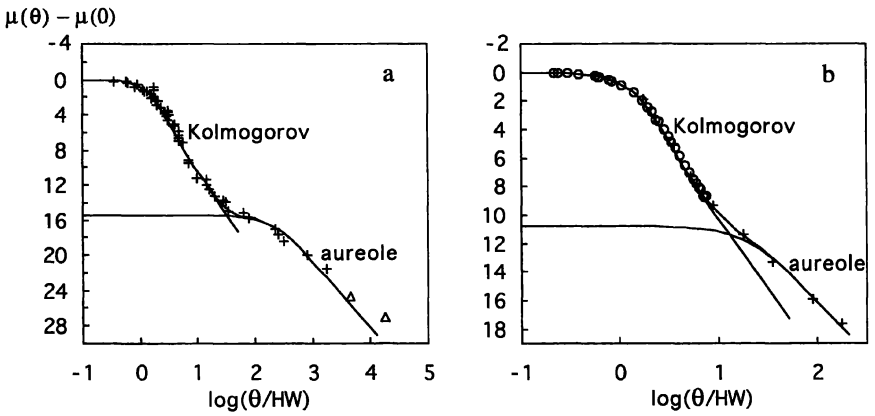

FIG. 4—The observed PSFs (symbols) fitted by the sum of a Kolmogorov profile plus an aureole given by Eq. (7): (a) King's photographic data (the two triangles are from measurements of the sky brightness near the Sun); (b) CCD data.

observations. Light scattering by very thin clouds could overwhelm such instrumental effects.

6. THE PSF STREHL RATIO

By its formal definition, the Strehl ratio of a PSF is the ratio of its central intensity to the central intensity of a fully diffraction-limited PSF of equal flux. When the diameter of the telescope aperture, D, is much larger than the Fried length r_0, atmospheric turbulence transforms a diffraction-limited Airy pattern into the characteristic long-exposure seeing disk. The total flux in an Airy pattern of unit central intensity (Strehl ratio $S\equiv 1$) can be shown to be

$$F_{\text{unit Airy}}=\frac{4}{\pi}\left(\frac{\lambda}{D}\right)^2. \tag{8}$$

The central intensity of a Moffat profile of total flux F [Eq. (6)] is

$$I_0(\text{Moffat})=\frac{4}{\pi}\frac{(2^{1/\beta}-1)(\beta-1)}{\text{FWHM}^2}F. \tag{9}$$

Substituting $F_{\text{unit Airy}}$ from Eq. (8) for F in Eq. (9) and using Eq. (5), one obtains

$$I_0(\text{Moffat})=1.702\frac{(2^{1/\beta}-1)(\beta-1)}{(D/r_0)^2}. \tag{10}$$

That central intensity is the Strehl ratio of the Moffat profile whose FWHM is that of the atmospheric PSF. The sum of an ($F_1=0.80$; $\beta_1=7$) and of an ($F_2=0.20$; $\beta_2=2$) profiles is a good representation of the Kolmogorov PSF (Fig. 3). With these parameters, the numerical constants in Eq. (9) combine to unity (in fact to 0.99) and, when $(D/r_0)\gg 1$,

$$S(D/r_0\gg 1)=(D/r_0)^{-2}. \tag{11}$$

Equation (11) obviously fails to yield the correct Strehl ratios for small values of D/r_0. It is also inappropriate when, for a given D/r_0, the wave-front structure function is modified by the corrective action of an adaptive optics system. An exact expression for S can be written as an integral of the structure function over the pupil, but this is somewhat inconvenient for rapid numerical evaluations. A number of closed-form approximations, whose range of applicability is limited, has been proposed (see below). A new expression, which is asymptotically exact for small and large values of D/r_0, and which quite accurately represents the Strehl ratios at intermediate values, both for natural and for partially compensated wave fronts, will now be derived.

Maréchal (1947) (see also Born and Wolf 1965) has shown that when the variance σ^2 of an aberrated wave front is small, for any structure function of the aberrations

$$S(\sigma^2\ll 1)=1-\sigma^2. \tag{12}$$

For Kolmogorov turbulence,

$$\sigma^2=\Delta_N(D/r_0)^{5/3}, \tag{13}$$

where $\Delta_N=1.030$ for a natural (long exposure, uncompensated) and 0.132 for a short-exposure (tilt-removed) PSF (Noll 1976).

TABLE 2
Strehl Ratios for Long and Short Exposures

D/r_0	S_{long}	S_{short}	$S_{\text{short}}/S_{\text{long}}$
0.0	1.000	1.000	1.00
0.1	0.978	0.997	1.02
0.5	0.741	0.948	1.28
1.0	0.445	0.844	1.90
2.0	0.175	0.594	3.38
3.0	0.089	0.369	4.17
3.5	0.067	0.285	4.23
4.0	0.053	0.218	4.10
5.0	0.035	0.128	3.64
7.0	0.019	0.051	2.76
10.0	0.009	0.021	2.18

Any general expression for S must reduce to the limiting forms given by Eqs. (11) and (12). The so-called "Maréchal extended approximation," $S=\exp(-\sigma^2)$, which does reduce to Eq. (12) and always remains positive, is often used, without reference to its source which this author has been unable to locate.

Exact numerical values of the normalized Strehl resolution $\mathscr{R}/\mathscr{R}_{\max}\equiv S(D/r_0)^2$ are given in Table I of Fried (1966b) for the long- and short-exposure cases. $\mathscr{R}/\mathscr{R}_{\max}$ is the central intensity of the PSF normalized to unity for an infinitely large, uncompensated telescope (Roddier et al. 1991). The corresponding Strehl ratios are found in Table 2, together with the Strehl gains $S_{\text{short}}/S_{\text{long}}$ produced by image stabilization, or tilt removal. These gains reach a maximum at $D/r_0=3.5$. A general expression for S should also closely fit these figures

It is clear that an equation of the form

$$S=\frac{1-e^{-k\sigma^{2n}}}{1+(D/r_0)^2}+e^{-\sigma^2} \tag{14}$$

always reduces to Eq. (11) for $k>0$, and also to Eq. (12) for $n>1$. Parenti (1992) indeed proposes a special case of Eq. (14) ($k=n=1$) to represent the tilt-removed Strehl ratio (see also Tyson 1994, Eq. (1) where, however, a sign error is present). The first term on the right of Eq. (14) can be thought of as the contribution of the PSF halo to the central intensity of a core *plus* halo profile, the core being a diffraction-limited "spike" whose central intensity is given by the Maréchal extended approximation, which is the second term. It is well known that under increasingly high levels of adaptive optics compensation, light removed from the broad seeing disk contributes to the growth of a diffraction-limited PSF core (Wang and Markey 1978; Roddier et al. 1991, Fig. 19). The parameters k and n can be adjusted to represent as well as possible the Strehl ratios in Table 2. It was found that $k=1/6$ and $n=5/3$ give quite acceptable results, as shown in Fig. 5. Tests with numerically calculated Strehl ratios for levels of corrections reducing Δ_N to as low a value as 0.01 gave equally satisfactory results, i.e., the correct Strehl ratio to within ± 0.02. The equation

$$S=\frac{1-e^{-1/6\sigma^{10/3}}}{1+(D/r_0)^2}+e^{-\sigma^2} \tag{15}$$

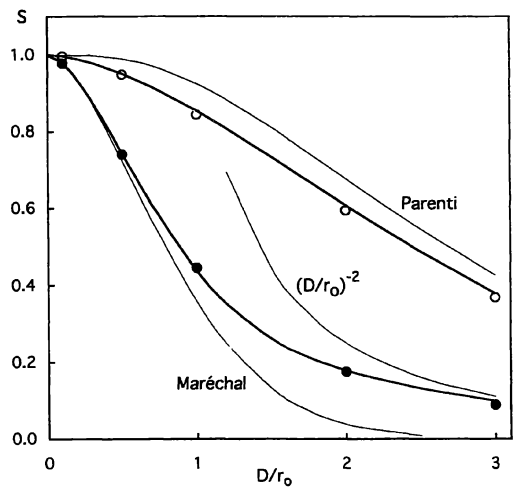

FIG. 5—The results of Eq. (14) with $k=1/6$ and $n=5/3$ (heavy lines) are compared to the exact Strehl values for natural (dots) and tilt-removed (open circle) turbulence. The thin lines show other approximations and required asymptotic behaviors (see text).

therefore provides a convenient and reasonably accurate estimate of the Strehl ratio of a PSF for any value of D/r_0 and for any level of wave-front compensation.

As a last test, Eq. (15) can be used to calculate the normalized Strehl resolution $\mathscr{R}/\mathscr{R}_{max}$ for increasing levels of wave-front compensation or, equivalently, of σ^2 reduction. Figure 6 shows the results; the curves are labeled by their coefficient Δ_N. They are in good agreement with similar curves based on rigorous calculations (Roddier 1990) reproduced in Roddier et al. (1991) (their Fig. 1) and whose levels of compensation correspond to the Δ_N values in Fig. 6.

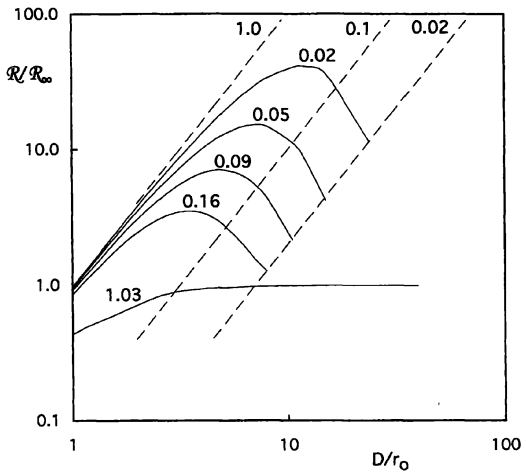

FIG. 6—Normalized Strehl resolution obtained from Eq. (15) as a function of (D/r_0) for various residual wave-front variances given in units of $(D/r_0)^{5/3}$ above each curve. Dashed lines are loci of constant Strehl ratios given by the upper labels.

7. CONCLUSION

Precise photometric measurements show that the shape of the inner stellar PSF produced by atmospheric turbulence agrees remarkably well with the one expected from a wave front whose structure function follows Kolmogorov statistics. A faint extended PSF aureole similar to the one described by King (1971) was also observed surrounding this inner PSF; it cannot result from turbulence and appears to be, in part, an instrumental effect. Its intensity can be strongly enhanced by the presence of hardly detectable cirrus clouds. Relatively simple yet accurate analytical representations of the PSF profiles have been developed. They can be useful for image simulation and analysis.

A new expression for the Strehl ratio of the PSF produced by a natural or by a partially compensated wave front was derived and tested against rigorous models. It was shown to yield reasonably accurate results for any value of the parameter (D/r_0) and for any level of compensation. Such an expression can be useful to quickly calculate the imaging performances of adaptive optics systems under various operating conditions.

The author is grateful to S. Demers, R. Doyon, I. King, D. Nadeau, and A. Tyson for access to, use, and discussions of their observational material. Discussions with and comments from J. Beckers, R. McClure, and F. Roddier are also gratefully acknowledged. This research was supported in part through grants from NSERC Canada and from Fonds FCAR, Québec.

REFERENCES

Beckers, J. 1993, ARAA, 31, 13
Beckers, J. 1995, in Scientific and Engineering Frontiers for 8–10 m Telescopes, ed. M. Iye and T. Nishimura (Tokyo, Universal Academy), p. 303
Born, M., and Wolf, E. 1965, Principles of Optics (Oxford, Pergamon), Chap. 9, p. 459
de Vaucouleurs, G. 1948, Ann. d'Astrophys., 11, 247
de Vaucouleurs, G. 1958, ApJ, 128, 465
Fried, D. L. 1965, JOSA, 55, 1427
Fried, D. L. 1966a, JOSA, 56, 410E
Fried, D. L. 1966b, JOSA, 56, 1372
Johnson, C. B. 1973, Appl. Opt., 12, 1031
King, I. R. 1971, PASP, 83, 199
King, I. R., and Hinrichs, E. L. 1967, PASP, 79, 226
Kormendy, J. 1973, AJ, 78, 255
Maréchal, A. 1947, Rev. d'Optique, 26, 257
Moffat, A. F. J. 1969, A&A, 3, 455
Noll, R. J. 1976, JOSA, 66, 207
Parenti, R. R. 1992, Lincoln Lab J., 5, 93
Roddier, C., and Roddier, F. 1993, in Proceedings of the Second International Conference on Planetary Systems: Formation, Evolution, and Detection, Waikoloa, Dec. 13–15, 1993
Roddier, F. 1981, Prog. Opt., 19, 109
Roddier, F. 1995, A&SS, 223, 109
Roddier, F., Northcott, M., and Graves, J. E. 1991, PASP, 103, 131
Roddier, N. 1990, Proc. SPIE, 1237, 668
Stetson, P. B. 1987, PASP, 99, 191
Stetson, P. B. 1994, Astronomy with the CFHT Adaptive Optics Bonnette, ed. R. Arsenault (Kamuela, HI, Canada–France–Hawaii Telescope Corp.), p. 72

Stetson, P. B., Davis, L. E., and Crabtree, D. R. 1990, in CCDs in Astronomy, ed. G. H. Jacoby, ASP Conf. Ser., 8, p. 289

Tatarski, V. I 1961, Wave Propagation in a Turbulent Medium (New York, McGraw-Hill), p. 269

Tyson, R. K. 1994, ICO-16 Conf. on Active and Adaptive Optics, ed. F. Merkle (Garching, ESO), p. 35

van de Hulst, H. C. 1952, in The Atmosphere of the Earth and Planets, ed. G. P. Kuiper (Chicago, University of Chicago Press), p. 69

van de Hulst, H. C. 1981, Light Scattering by Small Particules (New York, Dover)

Wang, J. Y., and Markey, J. K. 1978, JOSA, 68, 78

Woolf, N. J. 1982, ARAA, 20, 367